Journal of the European Ceramic Society 43 (2023) 2951–2957

Contents lists available at ScienceDirect

Journal of the European Ceramic Society

journal homepage: www.elsevier.com/locate/jeurceramsoc

Determining the interlaminar tensile strength of a SiC_f/SiC ceramic matrix composite through diametrical compression testing

C.D. Newton [a], S.P. Jeffs [a,*], L. Gale [b], S. Pattison [b], M.R. Bache [a]

[a] Institute of Structural Materials, Faculty of Science & Engineering, Swansea University, SA1 8EN, United Kingdom
[b] Rolls-Royce plc, P.O. Box 31, Derby DE24 8BJ, United Kingdom

ARTICLE INFO

Keywords:
Ceramic matrix composite
Inter laminar strength
Diametrical compression
Weibull distribution
Digital image correlation

ABSTRACT

Interlaminar tensile strength (ILTS) of a SiC_f/SiC Ceramic Matrix Composite (CMC) was determined through use of a diametrical compression test of disk geometries, with two geometries are investigated (Φ4.5 and Φ9 mm). Results are correlated with the fracture surface architecture, specifically relating to fibre tows. Due to the stochastic nature of ceramic material systems a Weibull distribution was implemented to understand the characteristic strength and distribution of the data sets for both disk geometries. Overall, a decrease in characteristic ILTS coupled with a narrowed distribution is observed for the Φ9 mm compared the Φ4.5 mm disk geometries due to the repeating unit cell size of the SiC_f/SiC CMC under investigation.

1. Introduction

SiC_f/SiC Ceramic Matrix Composites (CMCs) are considered a key material for high temperature structural applications, such as those required in aero-engines [1,2]. Their specific strength properties as well as maintaining their strength at temperatures up to 1250 °C means that improved thermal efficiencies, thrust-to-weight ratios and reduced emissions are possible for aero-engines. However, in order to realise CMCs into such applications, their mechanical performance under various loading conditions, such as ultimate strength, fracture resistance and fatigue tolerance, must be well understood. A particular area of concern is the delamination failure of CMCs materials under Mode I, Mode II and Mixed Mode loading conditions [3]. This type of failure is unusual in more traditional aero-engine materials, specifically nickel-based superalloys alloys, but common in composite materials since they are typically manufactured through assemblies of layers / plies. Therefore, separation between such layers under mechanical and thermal loading is prone to occur.

A variety of techniques have been applied to understand interlaminar properties of composites and CMC materials. For interlaminar shear strength (ILSS) the double notch shear test is a recognised method [4] that has been applied to Carbon-Carbon composites [5] and SiC CMCs [6]. For determining interlaminar tensile strength (ILTS), the developed techniques typically sit in two groupings. Firstly, those that implement transverse tensile loading of flat specimens, which can be square or button in shape, where the specimens are adhesively bonded to platens to enable loading [7] although such tests can have issues with edge effects and stress concentrations [5,8,9]. To mitigate these effects a modified button test [10] was developed using oversized test specimens relative to the platens, which resulted in a more reliable stress field and yielded higher ILTS than the standard geometry. A further challenge with these techniques is related to obtaining high temperature ILTS properties due to limitations related with the adhesive bonding. The second grouping uses curved specimens in a bending configuration, where the bending moment induces an out-of-plane tensile stress [11–14], while these methods produce a consistent stress field in comparison to aforementioned flat specimen techniques, concerns remain in terms of high temperature application and whether curved specimens are representative.

An alternate technique that falls outside of these groupings that can be used to determine ILTS of CMC materials is the diametrical compression test, a technique that has been applied to other inherently brittle material systems [15,16]. During the diametrical compression test a cylindrical disk specimen is exposed to a compressive load via two rigid platens [17]. Hertzian contact mechanics [18] can be applied to the diametrical compression test arrangement, under the assumptions that the material surfaces in contact and continuous, frictionless and it is only valid for small strains. Under these assumptions the largest magnitude principal stress is found to be the in-plane stress at the centre of the disk [19], which in the case of appropriately aligned CMCs would be the

* Corresponding author.
E-mail address: s.p.jeffs@swansea.ac.uk (S.P. Jeffs).

https://doi.org/10.1016/j.jeurceramsoc.2022.11.014
Received 15 June 2022; Received in revised form 31 October 2022; Accepted 6 November 2022
Available online 8 November 2022

ILTS. A schematic of the test setup in shown in Fig. 1a, with the in-plane stress, σ_x, is determined by Eq. (1) where, P is applied load, D_0 is the diameter of the disk and t is the thickness of the disk. Diametrical strain, ε_D is determined by Eq. (2) where, u, is the displacement in the loading direction. Fig. 1b, shows the key outcomes at fracture, with σ_{ILT} determined at the maximum load, P_F, and the diametrical fracture strain, ε_{Df}, determined from the displacement at fracture, u_f. A key advantage of the diametrical compression test is easily adapted for high temperature application [20] with the limitation arising only from the platen material.

$$\sigma_x = \frac{2P}{\pi \bullet D_0 \bullet t} \tag{1}$$

$$\varepsilon_D = \frac{u}{D_0} \tag{2}$$

This article investigates the ILTS of SiC_f/SiC CMCs at room temperature via diametrical compression testing across two disk geometries (Φ4.5 and Φ9 mm). The differences in ILTS between the two geometries as well as the spread within each of the tested geometries are correlated with the CMC architecture seen on the fracture plane. Additionally, due to the stochastic nature of CMCs, a Weibull distribution is applied to both disk geometries to determine a characteristic ILTS ($\sigma_{\theta,\ ILT}$) and failure statistics.

2. Materials and methods

2.1. Materials

The CMC material under investigated is a SiC_f/SiC system processed at Rolls-Royce High Temperature Composites inc. via a proprietary processing route. It consists of five harness satin woven Hi-Nicalon™ fibre bundles (or tows) orientated in a 0–90° architecture, with a boron nitride interphase and matrix phase formed via a combination of chemical vapour infiltration (CVI) and melt infiltration (MI). Further detail on the manufacturing process has been previously discussed [21]. In the first instance flat panels of approximate thickness 5 mm and dimensions 150 × 150 mm were manufactured, secondly, due to the level of scatter found in testing these thinner panels, thicker CMC panels of 150 × 150 × 10 mm were also manufactured for the purpose of this research.

2.2. Diametrical compression testing

Small disk specimens were extracted from the edge of the manufactured 150 × 150 × 5 mm and 150 × 150 × 10 mm flat panels, with the outer edges ground smooth. Disk specimens from the 5 mm thick panel measured Φ4.5 × 4 mm thick, and Φ9 × 7 mm from the 10 mm thick panels. Testing was performed at room temperature under monotonic position control using an Instron 6284 electric screw driven test frame. The test involved compressing the SiC_f/SiC disk laterally along the direction of the fibres between two stainless steel platens, as shown in Fig. 2. The resulting stress concentration along the central plane causes tension to be applied perpendicular to the loading direction and thus failure occurs between the laminates. To ensure consistent alignment of the CMC plies between tests, specimens were loaded using a microscope attachment to a CCD camera along with a removeable bespoke 3D printed alignment jig. A preload of 0.2 kN was applied to maintain position and alignment ahead of beginning the tests. Tests were run at three displacement rates: 0.0167 mm•s^{-1}, 0.005 mm•s^{-1} and 0.0001 mm•s^{-1} until ultimate failure, this was done to understand if there was any influence of test rate on ILTS. In addition, the lowest rate (0.0001 mm•s^{-1}) was implemented to help obtain successful Digital Image Correlation (DIC) data due to the rapid nature of failure. A total of 63 tests were performed, 38 of the Φ4.5 mm disks and 25 of the Φ9 mm disks.

2.2.1. Diametrical strain

Diametrical strain was determined across all tests through use of compliance corrected machine displacement. Data for the compliance correction was measured through compressing a small cylinder of platen material up to the load range required for the diametrical compression test. To corroborate the compliance corrected machine displacement, physical measurements of the disk specimen diameter parallel to the loading direction were taken pre and post-test. The diametrical fracture strain determined by the two methods was generally in agreement, typically ± 10%, as such diametrical strain determined from the compliance corrected machine displacement is presented throughout.

In addition, several tests employed DIC to enable strain monitoring across the entire surface of the disk specimen. DIC apparatus consisted of a LaVision Imager E-Lite5M CCD camera, blue LED illumination set, blue bandpass filters and Strainmaster controller. A speckle pattern was applied to the circular face of the disk specimen with standard spray paint using an airbrush and 0.5 mm nozzle. An initial image capture of the undeformed specimen was correlated and compared to subsequent images recorded at a rate of 5 Hz during the test to calculate absolute surface strains parallel to the transverse orientation, E_{xx}. Utilising an optimised pixel sub-set size, the localised strain could be determined at room temperature to an accuracy within 0.01%. Strain maps presented in this article have a colour gradation scale representing − 1% compression (black) to 5% tension (red). White areas indicate levels of strain beyond the nominally defined range, in this case signifying a large crack and ultimate failure of the material.

2.3. Fractography

Post-test fractography was conducted using a Keyence VHX-700 F microscope optical microscope. In instances where disks were not

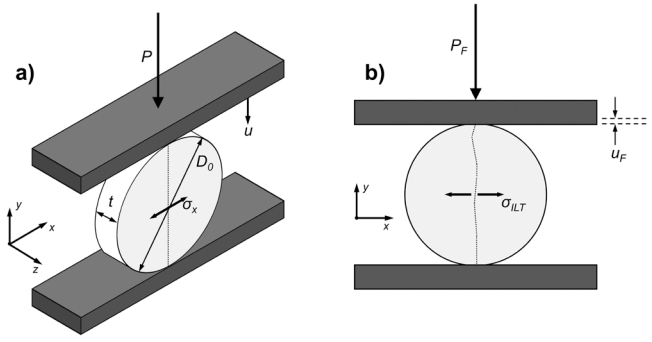

Fig. 1. Diametrical compression test schematic showing a) initial setup, key dimensions and key parameters, b) key outcomes at fracture.

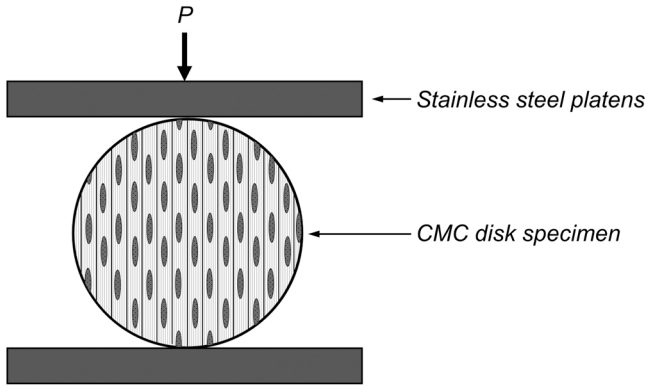

Fig. 2. Diametrical compression test arrangement showing the alignment of the CMC with the compressive loading direction.

wholly separated after testing, specimens were imaged prior to being mechanically split by use of forceps. Image segmentation of the fracture surface was carried out using Image J software. Fracture surfaces were segmented into three regions: longitudinal fibre tows (parallel with the loading plane), transverse fibre tows (perpendicular with the loading plane) and matrix phase.

3. Results & discussion

3.1. Diametrical stress vs. strain

Fig. 3 shows the characteristic response for in-plane stress, σ_x, against the diametrical strain, ε_D, for the diametrical compression tests, in this instance of a Φ9 mm disk specimen. The response can generally be thought of in two regions, the initial region sees a gradual increase in stress over the majority of the total observed diametrical strain, before transitioning into a more rapid acceleration in σ_x ahead of ultimate failure. During the initial region, the nature of the test arrangement means there is potential for localised damage at the contact region between platen and specimen, however, little evidence of this was visually observed. The key properties of σ_{ILT} and ε_{Df} are indicated on the curve and the small value in σ_x at the start of the curve is due to the initial preload that is applied to maintain the desired specimen alignment.

Interlaminar tensile strength, σ_{ILT}, vs. diametrical fracture strain, ε_{Df} for all diametrical compression tests performed is displayed in Fig. 4, along with the average, upper and lower bound σ_{ILT} values determined through a transverse tensile test load arrangement, specifically a standard button test [7] on the same material under investigation in this research. While the button data may underestimate the σ_{ILT} based on research into using a modified button test [10] it offers a sensible baseline for comparison for the σ_{ILT} values determined here through diametrical compression testing. A summary of results is provided in Table 1. Overall, the diametrical compression test results are within or above the standard button test data giving confidence in the technique and the determined σ_{ILT} values. For the Φ4.5 mm specimens the maximum and minimum σ_{ILT} was found to be 71.6 MPa and 19.7 MPa respectively, with the maximum and minimum values for the Φ9 mm specimens 51.9 MPa and 17.2 MPa respectively. The scatter of σ_{ILT} in the Φ4.5 mm specimens is shown to be significantly greater than that of the Φ9 mm specimens, both in terms of the calculated standard deviation and range between the maximum and minimum values. This increased scatter is primarily associated with the influence of specimen size [20], since the Φ4.5 mm specimens are too small in diameter to encompass a repeating unit cell (~8 mm) of the SiC_f/SiC CMC under investigation. This issue is partially combatted by the Φ9 mm specimens, which can now encompass a complete unit cell, and reduced scatter is clearly observed. Although, it must be considered that location of a unit cell and number of partial unit cells within a specimen is ultimately determined by the manufactured specimen location from a panel.

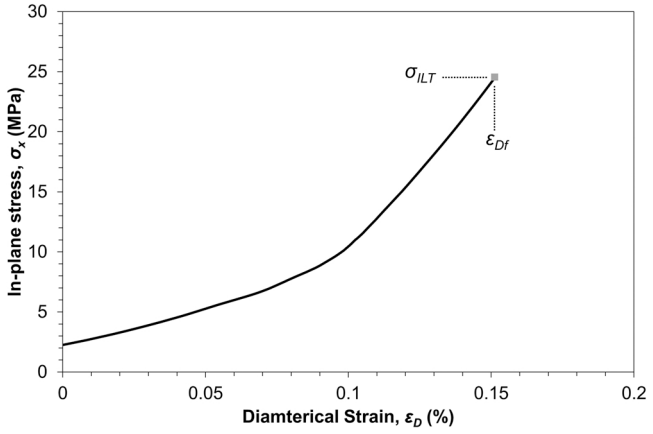

Fig. 3. Typical in-plane stress, σ_x, vs. diametrical strain, ε_D, response for diametrical compression testing of SiC_f/SiC CMCs.

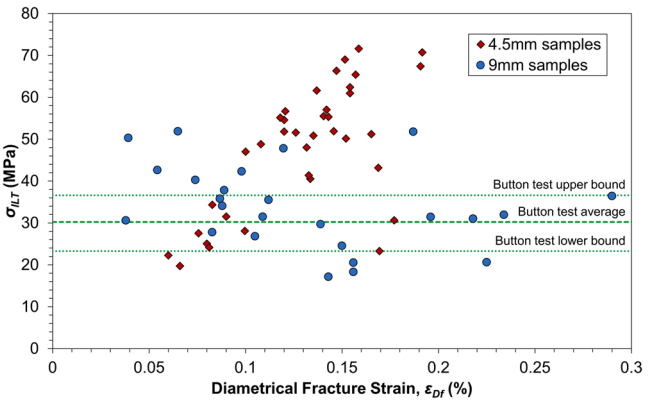

Fig. 4. Interlaminar tensile strength, σ_{ILT}, vs. diametrical fracture strain, ε_{Df} for all diametrical compression tests performed. Average, upper and lower bound σ_{ILT} values for the same SiC_f/SiC CMC determined through button testing have been plotted for comparison.

Table 1
Interlaminar tensile strength, σ_{ILT}, vs. diametrical fracture strain, ε_{Df} for all diametrical compression tests.

Test type	Sample diameter (mm)	Average, σ_{ILT} (MPa)	SD, σ_{ILT} (MPa)	Average, ε_{Df} (%)	SD, ε_{Df} (%)
Diametrical compression	4.5	48.1	13.1	0.15	0.05
Diametrical compression	9	33.8	10.3	0.12	0.06
Button[7]	–	30.2	–	–	–

3.2. DIC, Fractography and Image Analysis

Fig. 5 shows the transverse strain fields, E_{xx}, determined from DIC

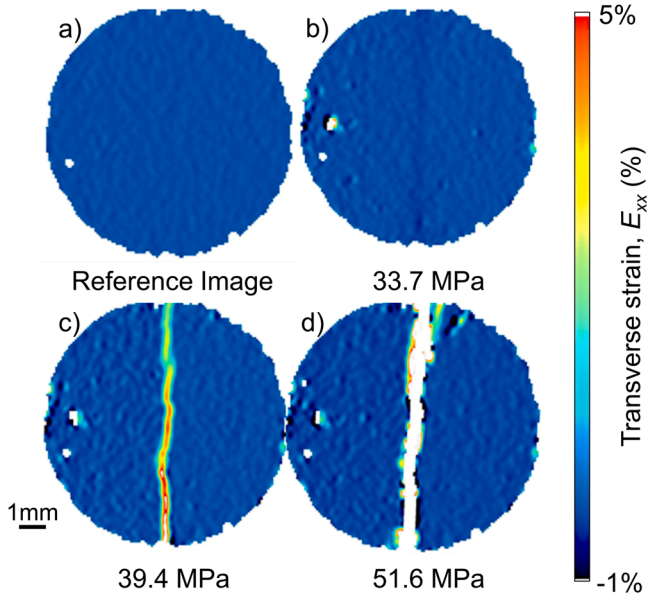

Fig. 5. Transverse strain (E_{xx}) fields determined from DIC during a diametrical compression test on a Φ9 mm disk where a) is the reference image, b) σ_x = 33.7 MPa, c) σ_x = 39.4 MPa and d) σ_{ILT} = 51.6 MPa.

during a diametrical compression test on a Φ9 mm disk. At the outset the DIC results corroborate the literature and show that the diametrical disk compression test is a valid technique for determining ILTS. Small levels of strain are apparent and a clear fracture path through the centre of the disk is observed due to the in-plane stress (σ_x) being the largest magnitude principal stress. The brittle nature of the ILT fracture is evident with all strain accumulation happening from 33.7 MPa (Fig. 5b), at which point little to no strain is shown, up to 39.4 MPa (Fig. 5c) ahead on ultimate failure at 51.6 MPa (Fig. 5d).

Fractography of a number of Φ4.5 mm specimens is shown in Fig. 6, indicating the fracture path location and the fracture surface architecture at $\sigma_{ILT} = 19.7$ MPa (Fig. 6a, b), 48.8 MPa (Fig. 6c, d) and 57.0 MPa (Fig. 6e, f), which are considered to be low, medium and high σ_{ILT} results respectively. Like the Φ4.5 mm specimens, fractography of a number of Φ9 mm specimens is shown in Fig. 7, indicating the fracture path location and the fracture surface architecture at $\sigma_{ILT} = 17.1$ MPa (Fig. 7a, b), 31.5 MPa (Fig. 7c, d) and 51.9 MPa (Fig. 7e, f), which are considered to be low, medium and high σ_{ILT} results respectively.

Across all specimens the fracture path is aligned parallel to the loading direction as is expected, although there are instances of multiple cracks at the contact surfaces such as that seen in Fig. 6e, which are attributed to compressive stresses that occur at these contact surfaces [15]. A perceptible pattern appears to emerge from the fracture surfaces in terms of the underlying structure, specifically the fibre architecture, this is not necessarily expected, due to the brittle nature of the crack propagation being through the SiC matrix. Nonetheless, for the low σ_{ILT} specimens there is a lack of longitudinal fibre tows (those parallel to the loading plane and perpendicular to σ_x) on the fracture surface which is not the case for the high σ_{ILT} specimens where an increase in longitudinal fibre tows is observed. In an attempt to quantify this potential trend image analysis on the fracture surfaces was performed, segmenting three regions: longitudinal fibre tows, transverse fibre tows (those perpendicular with the loading plane and parallel to σ_x) and matrix phase. Fig. 8 shows an example of this image segmentation analysis (Fig. 8a, b) and the relationship with σ_{ILT} (Fig. 8c) for the 25 Φ9 mm disks. The is no relationship from this analysis meaning that while the trend is observed optically it is not straightforward to quantify. This is thought to be because, the transverse tows are found to be prevalent on the fracture surface relative to the longitudinal tows in that the transverse tows cover the whole specimen thickness, whereas the longitudinal tows are typically seen between the transverse fibre tows. While this is to be expected since the transverse tows are aligned to σ_x, it creates a challenge for quantifiable fracture analysis.

3.3. Weibull distribution

As a result of the stochastic nature of CMCs, using average values for mechanical properties is often not appropriate and the distribution is of more importance. One distribution often applied to ceramic systems and CMCs is the Weibull distribution [22–24], which considers that the first sample to fail dominates the behaviour of the distribution [25]. The Weibull distribution is applied in this study to characterise σ_{ILT} determined from diametrical compression testing of SiC_f/SiC CMCs for both the Φ4.5 mm and Φ9 mm disk geometries. The Weibull probably density function (PDF) is defined by Eq. (3), and the Weibull cumulative density function is defined by Eq. (4):

$$f(x) = \frac{k}{\lambda}\left(\frac{x}{\lambda}\right)^{k-1} e^{-\left(\frac{x}{\lambda}\right)^{k}} \tag{3}$$

$$F(x) = 1 - e^{-\left(\frac{x}{\lambda}\right)^{k}} \tag{4}$$

where x is the mechanical property of interest, in this case σ_{ILT}, k is the Weibull Modulus and λ is the Weibull scale parameter. The scale parameter, λ, is taken as the Weibull characteristic strength, and is the σ_{ILT} value at $P_f = 63.2\%$, denoted as $\sigma_{\theta,\ ILT}$. The procedure to determine k and $\sigma_{\theta,\ ILT}$ is outlined. Firstly, the experimental σ_{ILT} values are ranked in ascending order termed, σ_i, where i is the consecutive number of the specimen from the ranked data set. A probability of failure (P_f) is then assigned to each value in using Eq. (5), where N is the total number of data points [26]:

$$P_f = \frac{i - 0.5}{N} \tag{5}$$

From here $ln(ln\ (1/1-\ P_f)$ and $ln\ (\sigma_{ILT})$ are calculated for each of the originally ranked data set and plotted as quantile-quantile (Q-Q) probability plots. From here, k and $\sigma_{\theta,\ ILT}$ can be determined. The Q-Q plots are shown in Fig. 9 for the Φ4.5 mm and Φ9 mm disk geometries, with the R^2 values exceeding 0.94 in each case indicating that the Weibull distribution fits the data sets well.

Figs. 10 and 11 show the Weibull CDF and PDF results respectively for the Φ4.5 mm and Φ9 mm disk geometries. The Weibull modulus, k, for the Φ4.5 mm specimens is determined to be 3.35 and for the Φ9 mm specimens 3.93. k offers a measure of distribution of the σ_{ILT}, here the slightly higher value indicates a marginally better consistency, which is this case here for the Φ9 mm specimens in comparison to the Φ4.5 mm specimens. This increase in k is credited to the increased specimen size which leads to increased consistency in terms of the repeating unit cell of

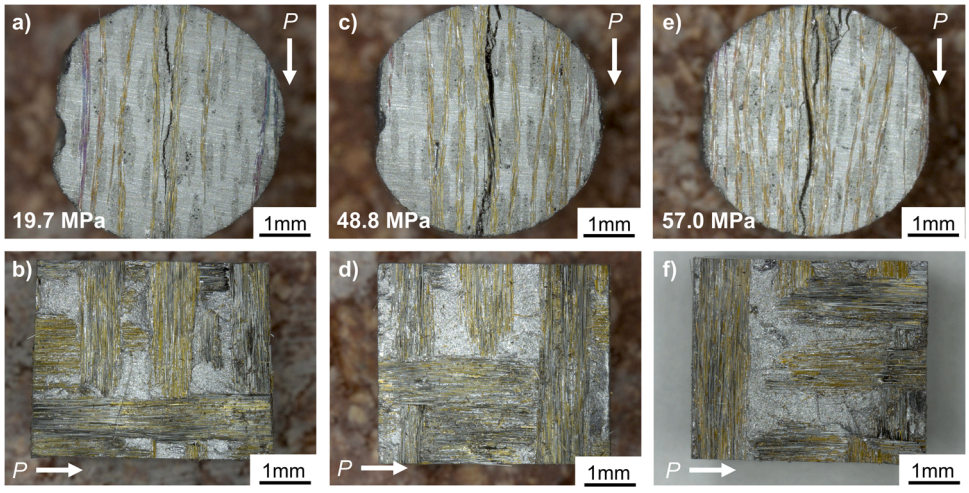

Fig. 6. Fractography of Φ4.5 mm specimens showing the fracture location on the disk surface and the fracture surface architecture over a range of interlaminar tensile strengths, σ_{ILT}.

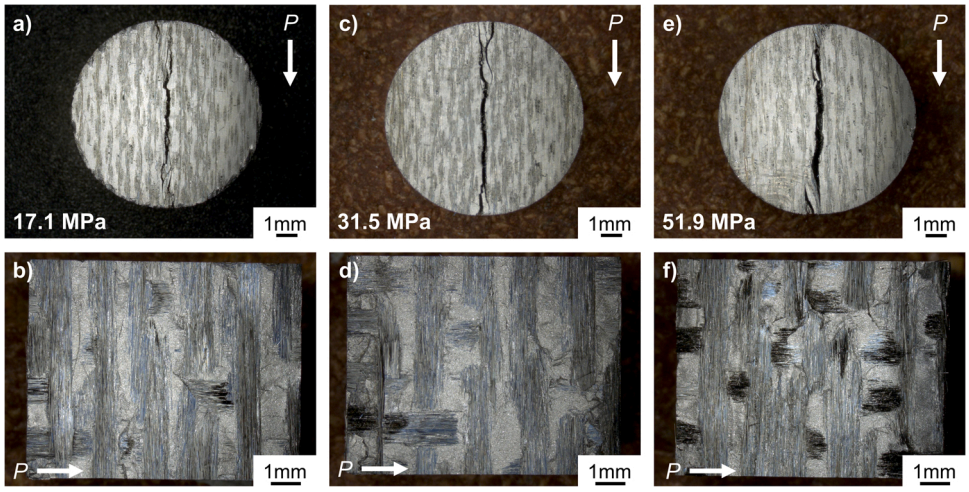

Fig. 7. Fractography of Φ9 mm specimens showing the fracture location on the disk surface and the fracture surface architecture over a range of interlaminar tensile strengths, σ_{ILT}.

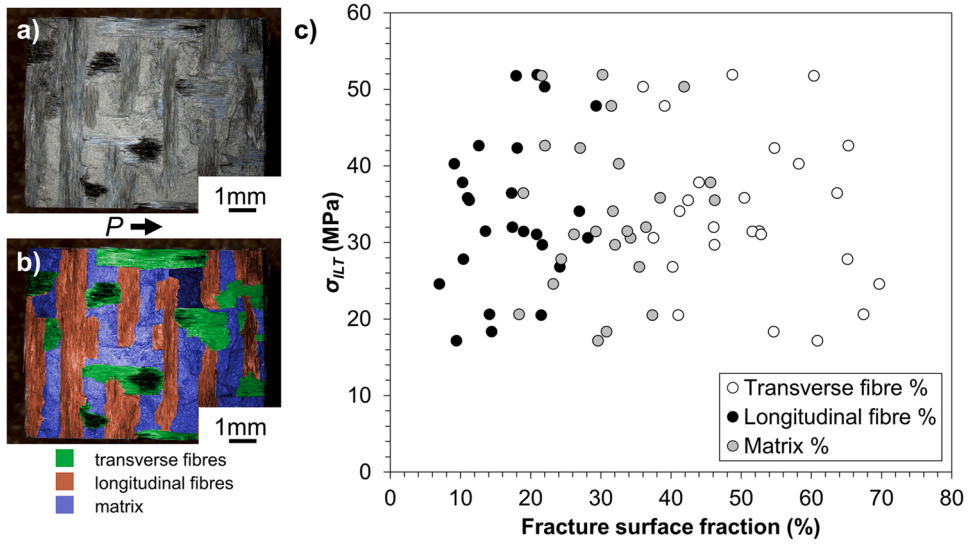

Fig. 8. (a, b) Example of fracture surface architecture and image analysis segmenting three regions: longitudinal fibre tows (parallel with the loading plane), transverse fibre tows (perpendicular with the loading plane) and matrix phase; (c) relationship between σ_{ILT} and the three analysed fractions for the Φ9 mm disks.

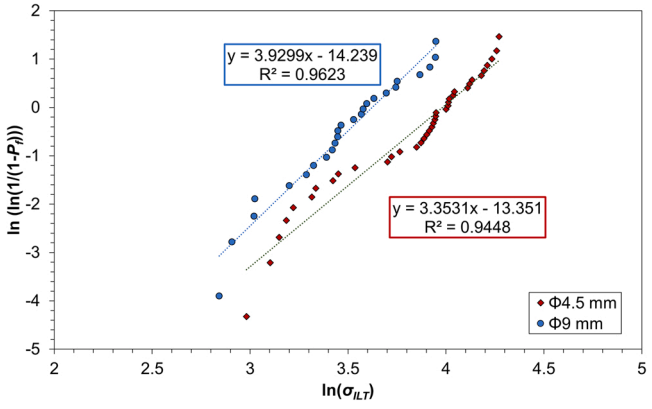

Fig. 9. Weibull *Q-Q* plots for the Φ4.5 mm and Φ9 mm diametrical disk experimental σ_{ILT} data sets.

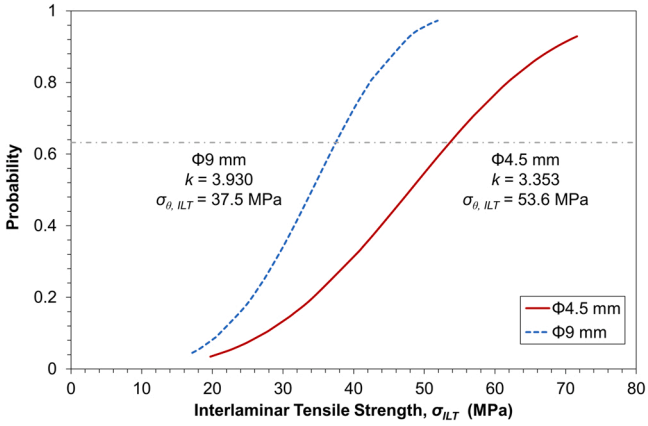

Fig. 10. Weibull CDF plots for the Φ4.5 mm and Φ9 mm disk geometries.

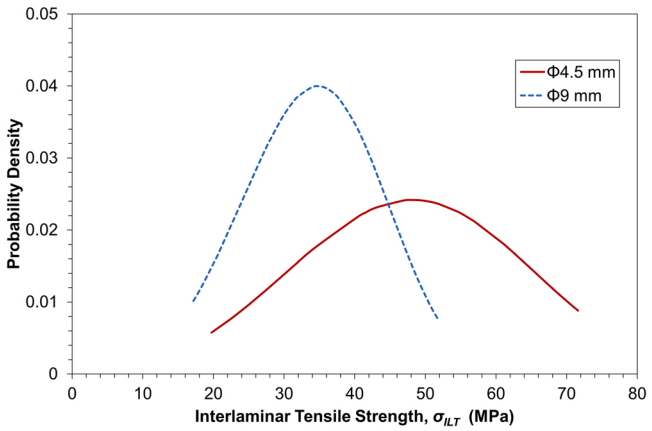

Fig. 11. Weibull PDF plots for the Φ4.5 mm and Φ9 mm disk geometries.

the SiC_f/SiC CMC material being tested. Nonetheless, it is important to mention that while an increase in k seen the Weibull modulus values for both specimen ($k < 4$), could be considered low for mechanical properties of SiC_f/SiC CMC materials [27–29], with $k > 10$ typically determined. This difference is understood to originate from two aspects, firstly, interlaminar separation type defects are significantly challenging in processing CMC material [30], which is related to why traditionally CVI and MI processing route has been used in these materials. Secondly, while the Φ9 mm disk geometry means that it is possible for a whole unit cell to be with a specimen the exact location of crossovers and where these points are relative to the in-plane stress, σ_x, is unknown. It is recognised that the modest increase seen in k between the two disk geometries could be attributed to the volume effect of Weibull analysis [31]. The characteristic strength, $\sigma_{\theta,\ ILT}$, is established as 53.6 MPa for the Φ4.5 mm specimens and 37.5 MPa for the Φ9 mm specimens. This decrease in $\sigma_{\theta,\ ILT}$ for the larger samples fits with the literature which shows a tendency for strength to decrease with increasing specimen volume [32]. However, this increase in $\sigma_{\theta,\ ILT}$ observed for the Φ4.5 mm specimens does come with an increase in distribution that has been discussed (Fig. 11). These points are associated with the likely structure in the smaller geometries, while it may be possible for the Φ9 mm specimens to encompass a repeating CMC unit cell (~8 mm). This is not the case for the Φ4.5 mm specimens which can only encompass a partial unit cell, where σ_{ILT} of partial unit cell, with no repeating crossover would be expected to be greater than that of a specimen does include such a repeating crossover. A summary of the Weibull parameters is given in Table 2.

4. Conclusions

In this article the diametrical compression test has been successfully used to investigate ILTS of a SiC_f/SiC CMC across two disk geometries, along with use of a Weibull distribution to characterise the data sets collected for each geometry, where the following conclusions can be drawn:

- The scatter observed in the σ_{ILT} results appears to correlate well with the architecture observed on the fracture surface with a larger number of longitudinal fibre tows found on the higher σ_{ILT} fracture surfaces, although quantitative image analysis of the fracture surface proved inconclusive.
- The characteristic strength from the Weibull distribution, $\sigma_{\theta,\ ILT}$ = 53.6 MPa for the smaller Φ4.5 mm disk geometry is found to be higher than for the Φ9 mm disk geometry ($\sigma_{\theta,\ ILT}$ = 37.5 MPa), while the Weibull modulus of k = 3.35 is slightly lower for the Φ4.5 mm compared to the Φ9 mm geometry (k = 3.95)

Table 2
Weibull parameters for diametrical compression testing of SiC_f/SiC CMCs with Φ4.5 mm and Φ4.5 mm disk geometries.

Sample diameter (mm)	k	$\sigma_{\theta,\ ILT}$ (MPa)	R^2
4.5	3.35	53.6	0.94
9	3.93	37.5	0.96

- This specimen volume effect is observed due to the repeating unit cell size of the material under investigation (~8 mm) relative to the diametrical compression test disk geometries. Therefore, ILTS data generated from small specimens must be carefully considered for any related future tests and their interpretation.

Declaration of Competing Interest

The authors declare that they have no known competing financial interests or personal relationships that could have appeared to influence the work reported in this paper.

Acknowledgments

The current research was funded via the IUK/ATI CEMTEC programme (113160). The provision of materials and technical support from Rolls-Royce plc. is gratefully acknowledged. Mechanical testing was performed by Swansea Materials Research & Testing (SMaRT).

References

[1] J.A. DiCarlo, Advances in SiC/SiC composites for aero-propulsion, Ceram. Matrix Compos. (2014) 217–235, https://doi.org/10.1002/9781118832998.ch7.
[2] N.P. Padture, Advanced structural ceramics in aerospace propulsion, Nat. Mater. vol. 15 (8) (2016) 804–809, https://doi.org/10.1038/nmat4687.
[3] R.S. Kumar, G.S. Welsh, Delamination failure in ceramic matrix composites: numerical predictions and experiments, Acta Mater. vol. 60 (6–7) (2012) 2886–2900, https://doi.org/10.1016/j.actamat.2012.01.053.
[4] ASTM C1292-22, Standard Test Method for Shear Strength of Continuous Fiber-Reinforced Advanced Ceramics at Ambient Temperatures, ASTM International, West Conshohocken, 2022.
[5] E. Lara-Curzio, D. Bowers, M.K. Ferber, The interlaminar tensile and shear behavior of a unidirectional C-C composite, J. Nucl. Mater. vol. 230 (3) (1996) 226–232, https://doi.org/10.1016/0022-3115(96)80018-3.
[6] Ö. Ünal, N.P. Bansal, In-plane and interlaminar shear strength of a unidirectional Hi-Nicalon fiber-reinforced celsian matrix composite, Ceram. Int vol. 28 (5) (2002) 527–540, https://doi.org/10.1016/S0272-8842(02)00006-8.
[7] ASTM C1468-19a, Standard Test Method for Transthickness Tensile Strength of Continuous Fiber-Reinforced Advanced Ceramics at Ambient Temperature, ASTM International, West Conshohocken, 2019.
[8] J.L. Abot, I.M. Daniel, Through-thickness mechanical characterization of woven fabric composites, J. Compos Mater. vol. 38 (7) (2004) 543–553, https://doi.org/10.1177/0021998304042394.
[9] A.K. Roy, A self-aligned test fixture for interlaminar tensile testing of two-dimensional carbon-carbon composites, J. Compos Mater. vol. 28 (4) (1994) 367–379, https://doi.org/10.1177/002199839402800406.
[10] J.H. Weaver, J. Yang, A.G. Evans, F.W. Zok, A modified test for measuring the interlaminar tensile strength of fiber-reinforced ceramic composites, Compos Sci. Technol. vol. 68 (1) (2008) 10–16, https://doi.org/10.1016/j.compscitech.2007.06.002.
[11] A. Makeev, G. Seon, Y. Nikishkov, E. Lee, Methods for assessment of interlaminar tensile strength of composite materials, J. Compos Mater. vol. 49 (7) (2015) 783–794, https://doi.org/10.1177/0021998314525979.
[12] J.S. Charrier, F. Laurin, N. Carrere, S. Mahdi, Determination of the out-of-plane tensile strength using four-point bending tests on laminated L-angle specimens with different stacking sequences and total thicknesses, Compos Part A Appl. Sci. Manuf. vol. 81 (2016) 243–253, https://doi.org/10.1016/j.compositesa.2015.11.018.
[13] W. Cui, T. Liu, J. Len, R. Ruo, Interlaminar tensile strength (ILTS) measurement of woven glass/polyester laminates using four-point curved beam specimen, Compos Part A Appl. Sci. Manuf. vol. 27 (11) (1996) 1097–1105, https://doi.org/10.1016/1359-835X(96)00071-1.
[14] Y. Wang, Z. Guan, X. Wang, F. Liu, T. Jiang, J. Xu, Mechanical properties and damage analysis of C/C–SiC curved beam under four-point bending: Experimental and numerical investigation, Ceram. Int. vol. 46 (16) (2020) 25646–25660, https://doi.org/10.1016/j.ceramint.2020.07.040.
[15] M. Scapin, L. Peroni, M. Avalle, Dynamic Brazilian test for mechanical characterization of ceramic ballistic protection, Shock Vib. vol. 2017 (2017), https://doi.org/10.1155/2017/7485856.

[16] P.M. Souto, M.A. Camerucci, A.G. Tomba Martinez, R.H.G.A. Kiminami, High-temperature diametral compression strength of microwave-sintered mullite, J. Eur. Ceram. Soc. vol. 31 (15) (2011) 2819–2826, https://doi.org/10.1016/j.jeurceramsoc.2011.07.034.
[17] M.H. Es-Saheb, A. Albedah, F. Benyahia, Diametral compression test: validation using finite element analysis, Int. J. Adv. Manuf. Technol. vol. 57 (5–8) (2011) 501–509, https://doi.org/10.1007/s00170-011-3328-0.
[18] H. Hertz, Ueber die Berührung fester elastischer Körper (on the contact of elastic so-lids), J. Reine Angew. Math. vol. 92 (1882) 156–171, https://doi.org/10.1515/crll.1882.92.156.
[19] N.H. Faisal, et al., Diametral compression test method to analyse relative surface stresses in thermally sprayed coated and uncoated circular disc specimens, Surf. Coat. Technol. vol. 357 (2018) (2019) 497–514, https://doi.org/10.1016/j.surfcoat.2018.10.053.
[20] C. Xu, X. Han, G. Cheng, S. Meng, H. Jin, Experimental study of ultra-high temperature interlaminar tensile strengths of 3D-needled C/C composites using the V-shaped notched specimen compression method, Mech. Mater. vol. 126 (2018) 26–35, https://doi.org/10.1016/j.mechmat.2018.07.003.
[21] O.G. Diaz, et al., Degradation mechanisms of SiC/BN/SiC after low temperature humidity exposure, J. Eur. Ceram. Soc. vol. 40 (12) (2020) 3863–3874, https://doi.org/10.1016/j.jeurceramsoc.2020.05.007.
[22] T.G. Aguirre, C.L. Cramer, V.P. Torres, T.J. Hammann, T.B. Holland, K. Ma, Effects of the addition of boron nitride nanoplate on the fracture toughness, flexural strength, and Weibull distribution of hydroxyapatite composites prepared by spark plasma sintering, J. Mech. Behav. Biomed. Mater. vol. 93 (2019) 105–117, https://doi.org/10.1016/j.jmbbm.2019.01.021.
[23] S. Flauder, N. Langhof, W. Krenkel, S. Schafföner, Size effect of carbon fiber-reinforced silicon carbide composites (C/C-SiC): Part 1 – bending load and statistical effects, J. Eur. Ceram. Soc. vol. 41 (14) (2021) 6805–6814, https://doi.org/10.1016/j.jeurceramsoc.2021.07.040.
[24] C.A. Klein, Characteristic strength, Weibull modulus, and failure probability of fused silica glass, Opt. Eng. vol. 48 (11) (2009), 113401, https://doi.org/10.1117/1.3265716.
[25] J.B. Wachtman, W.R. Cannon, and M.J. Matthewson, Mechanical Properties of Ceramics, Second Editon, 2009.
[26] ASTM C1239-13, Standard Practice for Reporting Uniaxial Strength Data and Estimating Weibull Distribution Parameters for Advanced Ceramics, ASTM International, West Conshohocken, 2018.
[27] J.C. McNulty, F.W. Zok, G.M. Genin, A.G. Evans, Notch-sensitivity of fiber-reinforced ceramic-matrix composites: effects of inelastic straining and volume-dependent strength, J. Am. Ceram. Soc. vol. 82 (5) (1999) 1217–1228, https://doi.org/10.1111/j.1151-2916.1999.tb01899.x.
[28] V. Calard, J. Lamon, A probabilistic-statistical approach to the ultimate failure of ceramic-matrix composites - Part I: experimental investigation of 2D woven SiC/SiC composites, Compos Sci. Technol. vol. 62 (3) (2002) 385–393, https://doi.org/10.1016/S0266-3538(01)00224-X.
[29] P.L.N. Murthy, N.N. Nemeth, D.N. Brewer, S. Mital, Probabilistic analysis of a SiC/SiC ceramic matrix composite turbine vane, Compos B Eng. vol. 39 (4) (2008) 694–703, https://doi.org/10.1016/j.compositesb.2007.05.006.
[30] Y. Gowayed, G. Ojard, E. Prevost, U. Santhosh, G. Jefferson, Defects in ceramic matrix composites and their impact on elastic properties, Compos B Eng. vol. 55 (2013) 167–175, https://doi.org/10.1016/j.compositesb.2013.06.026.
[31] A. Bhushan, et al., Weibull effective volumes, surfaces, and strength scaling for cylindrical flexure specimens having bi-modularity, J. Test. Eval. vol. 44 (5) (2016) 1978–1997, https://doi.org/10.1520/JTE20150301.
[32] M.R. Wisnom, Size effects in the testing of fibre-composite materials, Compos Sci. Technol. vol. 59 (1999) 1937–1957.